JACS JOURNAL OF THE AMERICAN CHEMICAL SOCIETY

Article

pubs.acs.org/JACS

Direct Synthesis of Inverse Hexagonally Ordered Diblock Copolymer/Polyoxometalate Nanocomposite Films

Thomas Lunkenbein,[†] Marleen Kamperman,*[,‡] Zihui Li,[∥] Carina Bojer,[†] Markus Drechsler,[§] Stephan Förster,[⊥] Ulrich Wiesner,[∥] Axel H. E. Müller,[§] and Josef Breu*[,†]

[†]Department of Inorganic Chemistry I, [§]Department of Macromolecular Chemistry II and [⊥]Department of Physical Chemistry I, University of Bayreuth, 95440 Bayreuth, Germany

[‡]Physical Chemistry and Colloid Science, Wageningen University, 6703 HB Wageningen, Netherlands

[∥]Department of Materials Science & Engineering, Cornell University, Ithaca, New York 14853, United States

Supporting Information

ABSTRACT: Nanostructured inverse hexagonal polyoxometalate composite films were cast directly from solution using poly(butadiene-block-2-(dimethylamino)ethyl methacrylate) (PB-b-PDMAEMA) diblock copolymers as structure directing agents for phosphomolybdic acid ($H_3[PMo_{12}O_{40}]$, H_3PMo). H_3PMo units are selectively incorporated into the PDMAEMA domains due to electrostatic interactions between protonated PDMAEMA and PMo^{3-} anions. Long solvophilic PB chains stabilized the PDMAEMA/H_3PMo aggregates in solution and reliably prevented macrophase separation. The choice of solvent is crucial. It appears that all three components, both blocks of the diblock copolymer as well as H_3PMo, have to be soluble in the same solvent which turned out to be tetrahydrofuran, THF. Evaporation induced self-assembly resulted in highly ordered inverse hexagonal nanocomposite films as observed from transmission electron microscopy and small-angle X-ray scattering. This one-pot synthesis may represent a generally applicable strategy for integrating polyoxometalates into functional architectures and devices.

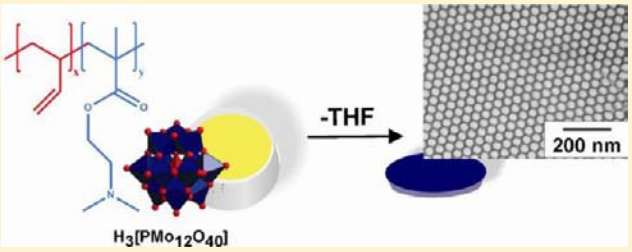

■ INTRODUCTION

Polyoxometalates (POMs) are early transition-metal oxide clusters of distinct charge, size, and shape.[1−5] In particular, Keggin-type heteropolyoxometalates (Keggin POMs) have found widespread application in fields of catalysis, electrochemistry, and host−guest chemistry as a consequence of their structural, chemical, and electronical diversity.[3,6−10] However, integration of Keggin POMs into ordered hybrid architectures remains challenging. When highly hydrophilic POMs are combined with hydrophobic organic structure directing agents, stabilization of the resulting hybrid materials in solvents that would allow controlled self-assembly is difficult. To meet this challenge, several strategies were developed to manipulate the surface properties of POMs.[11,12] For instance, phase transfer of POMs into hydrophobic solvents was accomplished by exchanging the counterions with cationic molecular surfactants generating so-called surfactant encapsulated polyoxometalate clusters.[13−21] Polarz et al. applied a smart approach where the structure directing surfactants were covalently attached to POM head groups.[22,23] In a separate step, these organophilic POMs could then be processed into thin hexagonally ordered films using, e.g., Langmuir−Blodgett techniques.

Discrete micellar, vesicular, and worm-like nanoobjects were obtained when amphiphilic diblock copolymers were used to generate hybrid materials.[24,25] With core-crosslinked diblock copolymers non-woven structures could be fabricated from discrete worm-like nanohybrids.[26]

Direct preparation of ordered nanostructured diblock copolymer/Keggin POM films as is well established, for instance, for inverse hexagonal TiO_2 films[27] has not been reported. Most likely, this is related to the difficulties encountered in stabilizing hybrid materials of strongly interacting Keggin POM anions and organic cations at high concentrations and high Keggin loadings.

Hexagonally packed cylinder structures (POMs segregated in the matrix surrounding cylinders, see Scheme 1) and bicontinuous morphologies would, however, be of particular interest because of increased robustness and proton conductivity.[28] Moreover, those morphologies can easily be transformed to catalytic active ordered metal carbide embedded in a porous carbon matrix.[29]

Here we describe a generally applicable strategy for producing inverse hexagonally ordered diblock copolymer/POM nanocomposite films by simple evaporation of the solvent similar to the evaporation induced self-assembly (EISA) processes reported earlier.[30,31]

Received: April 27, 2012
Published: July 3, 2012

Scheme 1. Illustration of One-Pot Direct Synthesis of PB-b-PDMAEMA/H_3PMo Nanocomposite Films[a]

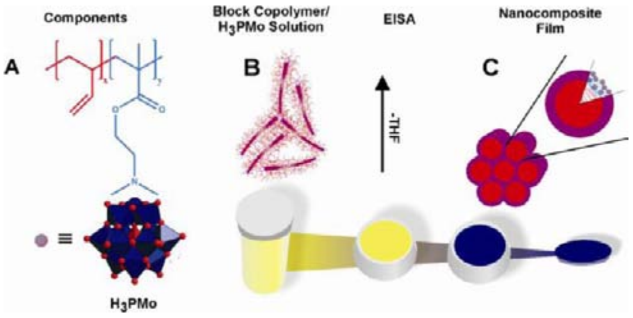

[a](A) Chemical structure of PB-b-PDMAEMA (top) and H_3PMo (bottom). DP: $x = 411$ and $y = 40$. (B) Micelle formation in solution with PB chains assuring solubility. (C) Inverse hexagonally ordered PB-b-PDMAEMA/H_3PMo nanocomposite film with PB cylinders in a PDMAEMA/H_3PMo matrix.

EXPERIMENTAL SECTION

Synthesis of Poly(butadiene-block-2-(dimethylamino)ethyl methacrylate) (PB-b-PDMAEMA) Diblock Copolymer. The diblock copolymer PB-b-PDMAEMA was synthesized by sequential living anionic polymerization in tetrahydrofuran (THF) as published elsewhere.[32] THF−gel permeation chromatography (GPC) was used to determine the molecular weight of the first block (polybutadiene, PB) using a PB calibration curve. The polydispersity index (PDI) of the diblock copolymer was determined by salt−GPC in the presence of 0.25 wt % of tributylammonium bromide and THF as eluent. In both cases, THF was HPLC grade (Aldrich), and measurements were conducted at room temperature (rt) and at flow rates of 0.5 mL/min. ^1H NMR was used to determine the chemical composition of the diblock copolymer. The resulting PB-b-PDMAEMA polymer had a molar mass of 29 kg/mol, a weight fraction of 22 wt % of PDMAEMA, and a PDI of 1.03.

Synthesis of Composites. Phosphomolybdic acid ($H_3[PMo_{12}O_{40}]$, H_3PMo, p.a.) was obtained from Aldrich. X-ray diffraction showed it to be a mixture of different hydrated phases. Therefore, it was recrystallized from water and stored at 86% relative humidity (RH) in order to ensure a defined stoichiometry.[33] Under these conditions, a crystalline material was obtained containing 27 water molecules per formula unit as confirmed by thermogravimetric analysis (Figure SI 1, Supporting Information). THF (p.a., Aldrich) was distilled to remove the stabilizer. In a typical block copolymer/H_3PMo nanocomposite synthesis, 0.1 g of the block copolymer was dissolved in THF (approximately 2 mL). The solution of the polymer was filtered (0.2 μm, Teflon) and added to a separate solution of H_3PMo in 3 mL of THF at rt under continuous stirring. After 30 min, the clear yellow solution was poured into a Teflon Petri dish (diameter: 3.2 cm) which was placed in an exsiccator kept at 32% RH and rt (Figure SI 2, Supporting Information). The Petri dish was covered by a hemispherical glass cap to control the evaporation rate of the solvent during EISA. Following this procedure, films with different H_3PMo content were prepared as listed in Table 2.

Characterization of the Composite Solution. For cryogenic transmission electron microscopy (cryo-TEM) studies, a drop of the solution in THF was put on a lacey carbon filmed TEM copper grid. Most of the liquid was removed with blotting paper, leaving a thin liquid film stretched over the lace. The specimens were instantly vitrified by rapid immersion into liquid nitrogen in a temperature-controlled freezing unit (Zeiss Cryobox, Zeiss NTS GmbH, Oberkochen, Germany). The frozen specimens were inserted in a Zeiss EM 922 OMEGA EF-TEM using a cryo transfer holder (CT3500, Gatan, München, Germany) and kept at temperatures around 90 K. The transmission electron microscope was operated at an acceleration voltage of 200 kV. Zeroloss filtered images ($\Delta E = 0$ eV) were taken under reduced dose conditions (100−1000 e/nm2). All images were registered digitally by a bottom-mounted CCD camera system (Ultrascan 1000, Gatan) combined and processed with a digital imaging processing system (Gatan Digital Micrograph 1.8).

Characterization of Inverse Hexagonally Ordered Films. Small-angle X-ray scattering (SAXS) data were collected at the Cornell High Energy Synchrotron Source (CHESS) applying a CCD 2-D detector. X-ray wavelengths of 1.378 and 1.252 Å were used, and the sample-to-detector distance was 352.02 and 371.58 cm, respectively. The fitting of the SAXS data was accomplished with the program SCATTER by Förster et al.[34,35]

Brightfield transmission electron microscopy (TEM) images were taken on a Zeiss CEM902 and a Zeiss EM922Omega operated at an acceleration voltage of 80 and 200 kV, respectively. As-synthesized composite films were microtomed under cryogenic conditions and placed on a lacey carbon filmed copper grid.

Fourier-transformed infrared (FTIR) data were collected on a Bruker IFS66 V using KBr pellets.

Powder X-ray diffraction (PXRD) patterns were obtained using nickel-filtered Cu Kα radiation ($\lambda = 1.54187$ Å) on a Bragg−Brentano-type diffractometer (XPERT-PRO, PANalytical B.V.) equipped with an X'Celerator Scientific RTMS detector. All patterns were analyzed using Panalytical's Highscore Plus software.

RESULTS AND DISCUSSION

Scheme 1 summarizes the one-pot route to inverse hexagonally ordered diblock copolymer/POM nanocomposite films. Well-ordered homogeneous nanocomposites can only be obtained if POMs are preferentially incorporated to one domain of the block copolymer and macrophase separation during self-assembly is prevented by assuring good solubility of the composite even at high polymer and POM concentrations. To meet these requirements, it was important to characterize the solution (Scheme 1B) to be able to optimize the process parameters.

Characterization of the Solution. PB-b-PDMAEMA was selected as structure directing agent (SDA). The amine function of the PDMAEMA block is sufficiently basic to be protonated by H_3PMo.[36] THF was selected as solvent since both the diblock copolymer and H_3PMo are soluble in it. Moreover, as will be discussed later, THF also is a good solvent for the second block (PB) which is not involved in the complex formation and thus assures the solubility of the PB-b-PDMEAMA/H_3PMo complex. PB_{411}-b-$PDMAEMA_{40}$ was synthesized by sequential living anionic polymerization. The subscripts denote the degree of polymerization (DP) of the corresponding blocks.

Both H_3PMo (diameter: 1.0−1.1 nm[2,21]) and PDMAEMA homopolymer ($\chi_{\text{PDMAEMA-THF}} = 0.003$, for details of the calculation of Flory−Huggins interaction parameters, χ, see the Supporting Information, section III) are highly soluble in THF.[37] First, a diblock copolymer solution in THF was added slowly to the H_3PMo solution in THF while stirring at rt. This solution stayed clear even at high composite concentrations (90 wt %) containing 83 wt % of H_3PMo (Figure SI 3, Supporting Information). After proton transfer, triply charged PMo^{3-} strongly interacted with the PDMAEMA cations.[38,39] These electrostatic interactions result in the formation of insoluble PDMAEMA/H_3PMo complexes.[38,39] When H_3PMo was added to a PDMAEMA homopolymer solution in THF instant precipitation of the complex was observed (Figure 1A). Contrary to this, no precipitate was formed when H_3PMo was added to PB-b-PDMAEMA. This is because the hydrophobic PB block is also highly soluble in THF ($\chi_{\text{PB-THF}} = 0.11$) and therefore capable of keeping the attached PDMAEMA/H_3PMo complex in solution (Figure 1B and Figure SI 4,

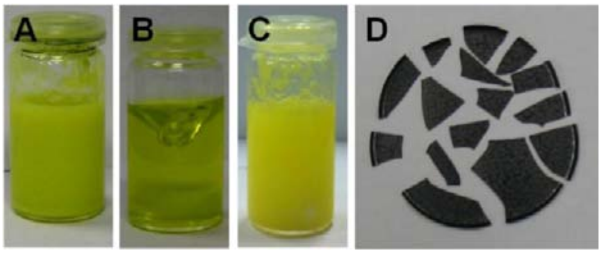

Figure 1. Photographs of (A) PDMAEMA homopolymer in the presence of H_3PMo in THF, (B) PB-b-PDMAEMA with H_3PMo in THF, and (C) PB-b-PDMAEMA with H_3PMo in acetone. In all cases, the H_3PMo content was 70 wt % related to the amount of diblock copolymer and the overall concentration of the PB-b-PDMEAMA/H_3PMo complex was 80 g/L. (D) As-synthesized PB-b-PDMEAMA/H_3PMo composite film as obtained for a H_3PMo loading of 70 wt %.

Supporting Information). For instance, acetone, a slightly poorer solvent for PB ($\chi_{\text{PB-acetone}}$ = 0.36), was already no longer capable of dissolving PB-b-PDMAEMA/H_3PMo complexes (Figure 1C). Furthermore, when the ratio of the degree of polymerization of PB to PDMAEMA approaches 1, immediate precipitation of the composite occurs (Figure SI 5A, Supporting Information), since the PB block is too short to render the PDMAEMA/H_3PMo complex soluble. Increasing the degree of polymerization to a ratio of 3 (Figure SI 5B, Supporting Information) resulted in a clear solution. Obviously, the PB block plays a key role in assuring the solubility during the self-assembly process. The type of mesophase formed is nevertheless controlled by the Florry−Huggins interaction parameter of the two blocks.

Micelle formation in THF solutions was systematically studied by cryo-TEM imaging as a function of H_3PMo loading of the PB-b-PDMEAMA/H_3PMo complex. Representative micrographs of three solutions containing complexes with decreasing PB-b-PDMAEMA/H_3PMo ratio are shown (3.23, 1.08 and 0.54) in Figure 2. The dimensions of the solution structures are given in Table 1. The contrast in TEM micrographs arises from electron density differences between PB and PDMAEMA/H_3PMo domains. The insoluble PDMAEMA/H_3PMo domains appear dark and PB domains grayish or undistinguishable from THF inclusions. Figure 2A corresponds to an H_3PMo content of 44 wt % showing spherical micelles consisting of solvophobic cores, i.e., PDMAEMA/H_3PMo, surrounded by solvophilic domains, i.e., PB.

The PDMAEMA/H_3PMo core diameter was 17 ± 3 nm and was stabilized by the PB chains. The PB-b-PDMAEMA/H_3PMo composite with a higher H_3PMo content of 70 wt % showed a 3D bicontinuous network (BCN) with typical 3- and 4-fold network junctions, loops, and end-caps (Figure 2B). The observed core diameter was slightly decreased (13 ± 3 nm) compared to the spherical micelles. This network structure has previously been observed for similar systems, such as surfactants, pure diblock copolymers, and diblock copolymer/POM systems.[25,40,41] Figure SI 6 (Supporting Information) shows a cryo-TEM image of PB-b-PDMAEMA/H_3PMo with a ratio of 1.08 at a thicker sample area of the vitrified film in which the interconnectivity in three dimensions is visible. Upon increasing the amount of H_3PMo with respect to PB-b-PDMAEMA, the solvophobic volume fraction increases. If one volume fraction is increased while keeping the other volume fraction constant (PB), at a certain point it will be favorable for the system to change morphology, for example, from a micelle to a network morphology.

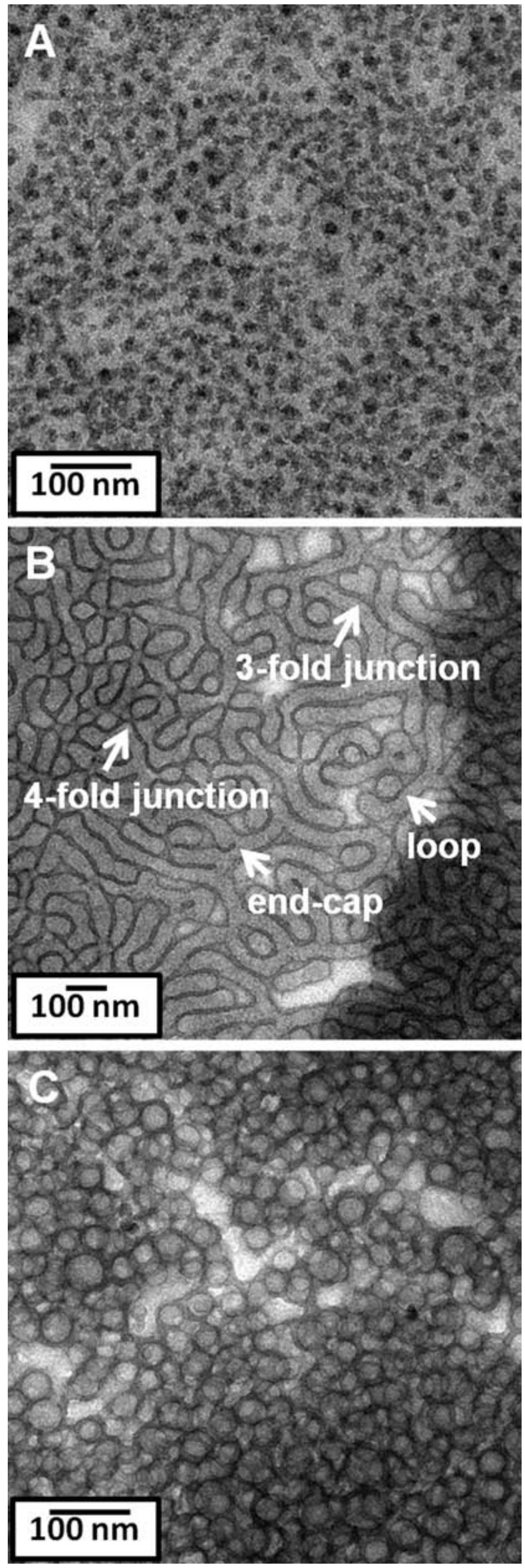

Figure 2. Cryo-TEM images in THF of nanostructures from varying PB-b-PDMAEMA/H_3PMo ratios: (A) 3.23, (B) 1.08, and (C) 0.54.

Further increase of H_3PMo content to 83 wt % resulted in a transition to vesicles (Figure 2C). The vesicles had

Table 1. Characteristics of PB-b-PDMAEMA/H_3PMo Complexes in THF As Observed by Cryo-TEM

PB-b-PDMAEMA/ H3PMo ratio	morphology	$d_c{}^a$/nm	$S_c{}^b$
3.23	spheroidal	16.93 ± 3.37	0.85
1.08	3D bicontinuous network	13.08 ± 2.89	0.65
0.54	vesicles	8.37 ± 1.67	0.42

[a]Core diameter of PB-b-PDMAEMA/H_3PMo domain in THF solution. [b]Stretching degree of PB-b-PDMAEMA/H_3PMo domain in THF solution.

PDMAEMA/H_3PMo wall thicknesses of 8 ± 2 nm and were fairly monodisperse with inner diameters of 22−30 nm. The sequence of morphologies observed in solution upon mixing H_3PMo with PB-b-PDMAEMA was in line with the expected preferential electrostatic interaction of H_3PMo with the PDMAEMA domains of the block copolymer inducing the phase transitions with increasing loadings.

The morphological changes resemble those previously documented for selective diblock copolymers[42,43] (with one solvophilic and one solvophobic block) and diblock copolymer/inorganic nanocomposites[44,45] and can be explained by molecular packing considerations. That is, with increasing H_3PMo content, the solvophilic and solvophobic volumes become more symmetric, leading to diminished chain stretching, S_c (see Table 1), and decreased interfacial curvature. Thus, by changing the solvophobic volume fraction with respect to the solvophilic volume fraction morphology transitions occur to optimize the balance between chain stretching and interfacial curvature solvent.

To follow the micelle transformation, dynamic light scattering experiments were conducted as presented in Figure SI 7, Supporting Information.

To quantitatively compare the results to known block copolymer phase behavior in selective solvents, effective volume fractions were calculated, taking PB as the solvophilic block and PDMAEMA/H_3PMo as the solvophobic block (Supporting Information, section VI). The resulting PDMAEMA/H_3PMo volume fractions of 0.27, 0.42, and 0.56 showing spherical micelles, networks, and vesicles, respectively, were considerably lower than what has been observed for selective, strongly segregated diblock copolymers, i.e., PB-b-PEO in water.[43] The volume fraction calculation was based on the assumption that the core domain density is the weighted average of the densities of PDMAEMA and H_3PMo. This assumption may be incorrect because the strong electrostatic interactions between PDMAEMA and H_3PMo may have led to a denser material. However, this would result in even lower volume fractions as compared to the reported values for PB-b-PEO in water. A more likely explanation is the high affinity of H_3PMo to bind THF molecules, which is described in the literature[46] and is consistent with our own observations (Supporting Information, section VI, Figures SI 8 and SI 9). Up to 20 THF molecules can adsorb to a single H_3PMo cluster, which is more than enough to explain the discrepancy in expected and observed volume fractions.[46] Whereas strongly segregated block copolymers have core domains that are free of solvent, the PDMAEMA/H_3PMo core domains may contain considerable amounts of THF (V_{THF} = 0.153 nm^3), which effectively increases the core volume fraction.

The characterization of PB-b-PDMAEMA/H_3PMo solutions in THF revealed considerable differences compared to the EISA process reported by Brinker et al.[30] While in EISA, the solvophilic block interacts with the inorganic material, here the solvophilic block stabilizes the inorganic/solvophobic block complex.

Film Casting. For film casting, the clear colloidal solutions were poured into a Teflon Petri dish, and volatiles were allowed to evaporate at rt and 32% RH. PB-b-PDMAEMA/H_3PMo composite films with eight different compositions were prepared (Table 2). At low H_3PMo content, films were transparent with green color. As the H_3PMo content increased, film colors gradually intensified into a dark blue. The color may be explained by a minute reduction and hydrolysis of H_3PMo to form the so-called molybdenum blues which have a very high extinction coefficient.[3,6] For all eight compositions, no precipitation was observed during casting. Moreover, films were homogeneous and did not show any signs of macrophase separation (see Figure 1D).

Nanocomposite films were characterized using combinations of FTIR spectroscopy, PXRD, SAXS, and TEM. FTIR spectra of PB-b-PDMAEMA diblock copolymer, the parent H_3PMo, and the PB-b-PDMAEMA/H_3PMo nanocomposites are shown in Figure 3A and Figure SI 10, Supporting Information. H_3PMo shows four characteristic bands, which are the fingerprint of the Keggin structure.[47,48] There are four kinds of oxygen atoms in H_3PMo (O_a, oxygen in PO_4 tetrahedron; O_d, terminal oxygen

Table 2. PB-b-PDMAEMA/H_3PMo Composites

sample	Keggin	wt % Keggin	block copolymer	H^{+a} (N)	r^b	M^c	$d_{spacing}{}^d$ (nm)	A^e (nm)	B^f (nm)	$f_{S,calc}{}^g$	$f_{s,TEM}{}^h$
POM1	H_3PMo	28	PB-b-PDMAEMA	0.46	6.52	M/D	31	nd[i]	nd	0.22	nd
POM2	H_3PMo	44	PB-b-PDMAEMA	0.93	3.23	M/D	29	nd	nd	0.27	nd
POM3	H_3PMo	54	PB-b-PDMAEMA	1.39	2.16	M/D	nd	nd	nd	0.31	nd
POM4	H_3PMo	61	PB-b-PDMAEMA	1.85	1.62	Hex	42	28.9 ± 2.7	7.9 ± 1.1	0.35	0.44
POM5	H_3PMo	70	PB-b-PDMAEMA	2.78	1.08	Hex	45	32.4 ± 2.5	10.2 ± 1.7	0.42	0.48
POM6	H_3PMo	76	PB-b-PDMAEMA	3.71	0.81	Hex	51	35.6 ± 2.8	9.2 ± 2.1	0.47	0.43
POM7	H_3PMo	80	PB-b-PDMAEMA	4.63	0.65	Hex/D	45	32.0 ± 3.9	6.8 ± 1.5	0.52	0.38
POM8	H_3PMo	83	PB-b-PDMAEMA	5.59	0.54	Hex/D	31	nd	nd	0.56	nd
POM9	H_3PMo	70	PB-b-P2VP	1.57	1.91	Hex	39	27.0 ± 1.6	8.98 ± 1.1	0.46	0.49
POM10	H_3PW	79	PB-b-P2VP	1.61	1.86	Hex	41	29.9 ± 2.1	9.11 ± 1.3	0.46	0.47

[a]Molar ratio of H^+ to DMAEMA units. [b]Molar ratio of DMAEMA units to H_3PMo. [c]Morphology of the mesostructured films: M, micellar; D, disordered; Hex, inverse hexagonal. [d]Determined from SAXS measurements. [e]PB cylinder diameter as obtained from TEM micrographs. [f]PDMAEMA/H_3PMo matrix thickness as obtained from TEM micrographs. [g]Calculated solvophobic volume fraction (Supporting Information, section V). [h]Solvophobic volume as obtained by TEM measurements. [i]Not distinguished.

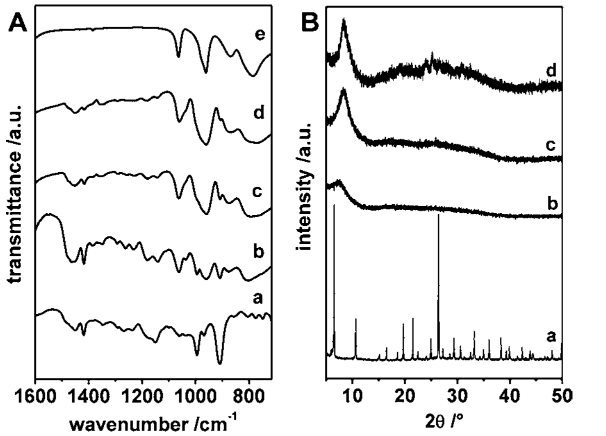

Figure 3. FTIR spectra (A) and PXRD patterns (B) of (b) POM2 (44 wt %), (c) POM5 (70 wt %), and (d) POM8 (83 wt %). For comparison, FTIR spectra of PB-b-PDMAEMA (Aa), parent H_3PMo (Ae), and the PXRD pattern of H_3PMo (Ba) are given.

atom to Mo; O_b, corner sharing oxygen; O_c, edge sharing oxygen) giving rise to characteristic bands at ν_{as} (Mo−O_d) 963 cm^{-1}, ν_{as} (Mo−O_b−Mo) 870 cm^{-1}, ν_{as} (Mo−O_c−Mo) 785 cm^{-1}, and ν_{as} (P−O_a) 1065 cm^{-1} (Figure 3Ae). The FTIR spectra of all nanocomposite films (POM1−8) were in good agreement with a superposition of the spectra of parent H_3PMo and PB-b-PDMAEMA polymer, suggesting that the Keggin structure stayed intact upon nanocomposite formation. A summary of observed peak positions of the various materials is given in Table SI 3 (Supporting Information).

The slight shift in wavenumbers observed for both Mo−O−Mo vibrations (corner and edge shared) is likely due to a change in the environment of the Keggin anions incorporated in the PDMAEMA block. Thus the shift in the frequencies indicated Coulomb interactions between PB-b-PDMAEMA and H_3PMo.

PB-b-PDMAEMA/H_3PMo nanocomposite films were amorphous, and PXRD patterns showed no peaks being characteristic for the parent crystalline H_3PMo (Figure 3B and Figure SI 11, Supporting Information), which again suggested a homogeneous dispersion of H_3PMo in the polymer matrix.

Structural assignment of the nanocomposite films was accomplished by a combination of SAXS measurements (only for selected samples, Figure 4) and TEM images (Figure 5). The SAXS traces of POM1 (28 wt %) and POM2 (44 wt %) (Figure 4A,B) showed broad first order peaks centered around values of the scattering wave vector q corresponding to a d-spacing of approximately 31 and 29 nm, respectively, indicating the absence of long-range order. SAXS patterns obtained for POM4−POM7 (Figure 4C−F and Figures SI 12 and SI 13, Supporting Information) exhibited distinguishable higher order reflections indicative of cylinders packed in a hexagonal lattice. The main peaks corresponded to d-spacings of 42, 45, 51, and 42 nm for samples POM4, 5, 6, and 7, respectively. Note that the d-spacing first increased with increasing H_3PMo content but then decreased again. This unexpected behavior will be discussed later. The scattering curve of POM8 (83 wt %, Figure 4G) possessed one broad, unstructured higher order reflection at angular position of 2 of the first order maximum, which is typical for short-range-ordered structures. The broad first-order maximum corresponded to a d-spacing of 31 nm.

Bright-field TEM micrographs (Figure 5) of the nanocomposites corroborated the structural assignments based on

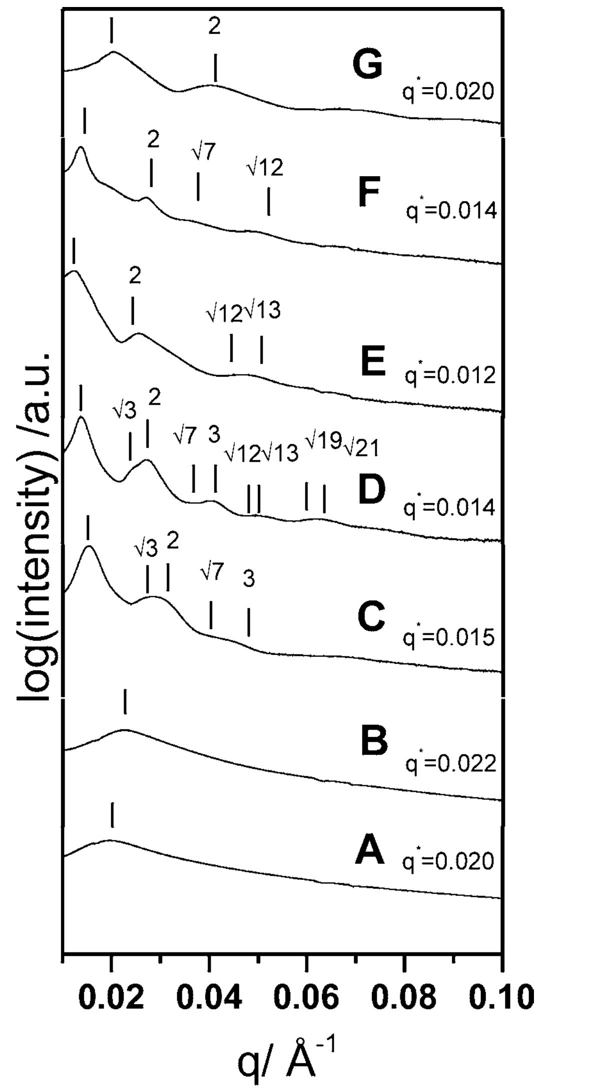

Figure 4. SAXS patterns of PB-b-PDMAEMA/H_3PMo nanocomposites: (A) POM1 (28 wt %), (B) POM2 (44 wt %), (C) POM4 (61 wt %), (D) POM5 (70 wt %), (E) POM6 (76 wt %), (F) POM7 (80 wt %), and (G) POM8 (83 wt %). The ticks denote the expected positions for hexagonal ordered cylinders.

SAXS experiments. For POM2 (Figure 5A), micellar disordered mesostructures were observed. Highly ordered hexagonally packed light cylinders in a dark matrix were found for POM4 and POM5 (Figure 5B,C), which translates to PB cylinders in a PDMAEMA/H_3PMo matrix. Further increase of the H_3PMo loading led to small regions with less order for POM6 and POM7 (Figure 5D,E), while for POM8 a further significant decrease of order was observed (see Figure 5F). In order to understand the trends of d-spacings observed by SAXS, the volume fractions of PB- and PDMAEMA/H_3PMo-blocks were determined from TEM images ($f_{s,TEM}$, see Table 2) for the inverse hexagonally ordered nanocomposite films and compared with calculated ($f_{s,calc}$) volume fractions (for calculation details see the Supporting Information section VI).

In line with the SAXS observations, $f_{s,TEM}$ first increased with increasing H_3PMo loading and then decreased again. As described above, H_3PMo is expected to preferentially enter the PDMAEMA domains. Therefore, increasing the H_3PMo content is expected to increase the solvophobic volume fraction (see $f_{s,calc}$ in Table 2, which is calculated on the basis of this

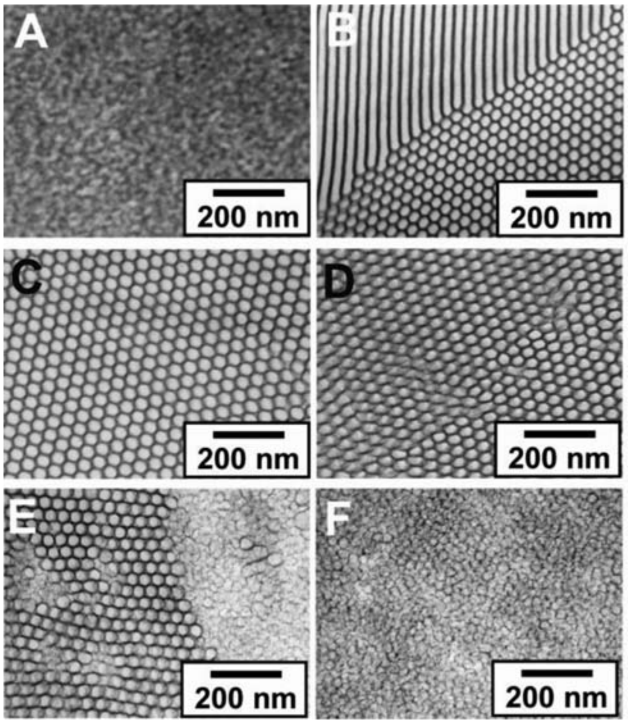

Figure 5. Representative bright-field TEM images of the as-synthesized PB-b-PDMAEMA/H_3PMo nanocomposites: (A) POM2 (44 wt %), (B) POM4 (61 wt %), (C) POM5 (70 wt %), (D) POM6 (76 wt %), (E) POM7 (80 wt %), and (F) POM8 (83 wt %).

assumption). However, at a certain stoichiometry, when the number of H_3PMo exceeds the number of DMAEMA units (r = DMAEMA/H_3PMo < 1, Table 2), the solvophobic volume fraction and the diameter of the cylinders for POM7 decreases. There are two possible explanations:

(1) Additional H_3PMo still enters the DMAEMA block and stronger hydrogen bonding resembling the crystalline state induces denser packing.

(2) PDMAEMA domains cannot accommodate additional H_3PMo, and it may become more favorable for H_3PMo to segregate to the interface.

Macrophase separation could be excluded for the following reasons: TEM images of the hybrids did not show completely disordered regions. Larger segregated H_3PMo particles would be expected to be easily spotted by the good z-contrast. Nanocomposite suspensions were transparent even at high concentrations, indicating that no light-scattering larger H_3PMo aggregates were formed. Moreover, macrophase separation could not explain the decrease in domain size which was observed in TEM and SAXS data for POM 7 and POM 8 and which cannot be regarded as insignificant and/or caused by peak broadening due to macrophase separation. Although POM units were not designed to go to the interface it is common and well-known for any particles to segregate to the interface (Pickering effect).[49,50]

Segregation to the interface leads to a decrease in interfacial tension and a corresponding decrease in domain size, allowing the stretching of the blocks to be decreased.[51−53] Since segregation to the interface is expected to be detrimental to ordering, the experimental observations (compare Figure 5C−F) are more in line with the second reasoning.

A second observation resembled solution behavior inasmuch as morphologies were obtained for smaller solvophobic volume fractions than expected from molecular packing arguments. It appeared that inverse hexagonal cylinders were obtained for unusual large PB volume fractions ranging from 0.51 to 0.66. Following the same line of argument discussed previously, relatively strong adsorption of THF to H_3PMo lead to temporarily swelling of the PDMAEMA/H_3PMo domains, thereby increasing the PDMAEMA/H_3PMo volume fraction. Free THF in the solvophilic PB-block is expected to evaporate first, while the PDMAEMA/H_3PMo domains remain swollen. Consequently, the volume fraction of the PB block at intermediate stages of the EISA where the hexagonal morphology develops will be much smaller as the volume fraction determined for fully dried, solvent free nanocomposite samples investigated by TEM. When finally the PDMAEMA/H_3PMo domains shrink upon evaporation of adsorbed THF, the mobility is already significantly reduced. Therefore, the system can only rearrange on a very local scale and the hexagonal morphology is retained. This might explain why inverse hexagonal morphologies with PB cylinders in a PDMAEMA/H_3PMo matrix were obtained for rather large $f_{s,TEM}$ of the PB block. Indirect proof for the shrinkage of PDMAEMA/H_3PMo domains at the final stages of film formation, is given by TEM micrographs at higher magnifications, which show light areas in the matrix at the corner of the hexagons, as depicted in Figure 6. It appears that these light

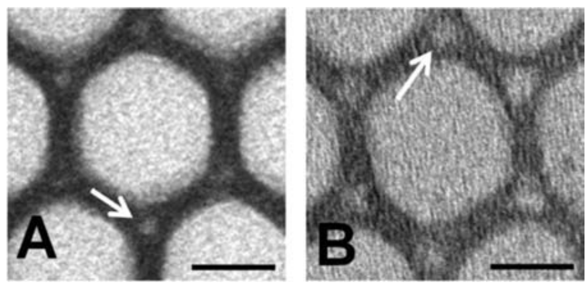

Figure 6. High-resolution TEM images of hexagonal mesostructures for (A) POM5 and (B) POM9. The arrows denote areas with low-electron densities within the matrix. The scale bars are 20 nm.

areas are voids induced by drying. It is obvious that the formation of voids is energetically unfavorable. However, voids are not uncommon and have been reported for inverse hexagonal arrays of lipids and charged surfactants.[54,55]

Finally we illustrate the general applicability of this novel approach for producing block copolymer/heteropolyoxometalate nanocomposites. Hexagonally ordered mesostructured films were also obtained applying a different block copolymer (poly(butadiene-block-2-vinylpyridine) (PB_{411}-b-$P2VP_{75}$) (POM9) or other HPAs like phosphotungstic acid ($H_3[PW_{12}O_{40}]$, POM10) (Table 1 and Figure SI 14, Supporting Information).

■ CONCLUSION

In summary, we presented a general one pot synthesis toward highly ordered inverse hexagonal block copolymer/heteropolyoxometalate nanocomposites. PB-b-PDMAEMA was chosen as SDA with a short ionizable block and a long solvophilic PB block. H_3PMo protonates the polymer and the polyanions selectively enter the PDMAEMA units. Macrophase separation was never observed. The PB-b-PDMAEMA/H_3PMo complex remains dissolved in THF even at high concentrations and H_3PMo loadings. At optimized H_3PMo loadings, inverse hexagonal mesophases were obtained by EISA. The general applicability of the method for mesostructuring was proven by extending it to other block copolymers and HPAs.

■ ASSOCIATED CONTENT

Ⓢ Supporting Information

Detailed equations, Tables SI 1−SI 3, and Figures SI 1−SI 14. This material is available free of charge via the Internet at http://pubs.acs.org.

■ AUTHOR INFORMATION

Corresponding Author

josef.breu@uni-bayreuth.de; marleen.kamperman@wur.nl

Notes

The authors declare no competing financial interest.

■ ACKNOWLEDGMENTS

This work was supported by the Deutsche Forschungsgemeinschaft (DFG) within the Collaborative Research Center (SFB) 840 (A7). T.L. thanks the international graduate school of the ENB "Structures, Reactivity and Properties of Metal Oxides" for a fellowship. M.K. was supported by The Netherlands Organization for Scientific Research (NWO, VENI-700.10.404). Z.L. was supported by the U.S. Department of Homeland Security under Cooperative Agreement No. 2009-ST-108-LR0004. The X-ray equipment was supported by Department of Energy Grant No. DEFG-02-97ER62443. CHESS was supported by the NSF and NIH-NIGMS via DMR-0225180.

■ REFERENCES

(1) Berzelius, J. J. *Pogg. Ann. Phys. Chem* **1826**, *6*, 369−380.
(2) Pope, M. T. *Heteropoly and Isopoly Oxometalates*: Springer-Verlag: Berlin, 1983; pp 15−32.
(3) Pope, M. T.; Müller, A. *Polyoxometalate Chemistry From Topology via Self-Assembly to Apllications*: Kluwer Academic Publishers: Dordrecht, 2001; pp 69−135.
(4) Johannson, G. *Acta Chem. Scand.* **1960**, *14*, 771−773.
(5) Keggin, J. F. *Nature* **1933**, *131*, 908−909.
(6) Moffat, J. B. *Metal-Oxygen Clusters - The Surface and Catalytic Properties of Heteropoly Oxometalates*; Kluwer Academic/Plenum Publishers: New York, 2001; pp 175−286.
(7) Katsoulis, D. E. *Chem. Rev.* **1998**, *98*, 359−387.
(8) Nomiya, K.; Murasaki, H.; Miwa, M. *Polyhedron* **1986**, *5*, 1031−1033.
(9) Misono, M. *Catal. Rev. Sci. Eng.* **1987**, *29*, 269−321.
(10) Pope, M. T.; Müller, A. *Angew. Chem., Int. Ed.* **1991**, *30*, 34−48.
(11) Long, D. L.; Tsunashima, R.; Cronin, L. *Angew. Chem., Int. Ed.* **2010**, *49*, 1736−1758.
(12) Song, Y. F.; Long, D. L.; Ritchie, C.; Cronin, L. *Chem Rec.* **2011**, *11*, 158−171.
(13) Kurth, D. G.; Lehmann, P.; Volkmer, D.; Cölfen, H.; Koop, M. J.; Müller, A.; Du Chesne, A. *Chem.—Eur. J.* **2000**, *6*, 385−393.
(14) Li, H.; Qi, W.; Li, W.; Sun, H.; Bu, W.; Wu, L. *Adv. Mater.* **2005**, *17*, 2688−2692.
(15) Li, W.; Bu, W.; Li, H.; Wu, L.; Li, M. *Chem. Commun.* **2005**, 3785−3787.
(16) Wang, Y. L.; Li, W.; Wu, L. X. *Langmuir* **2009**, *25*, 13194−13200.
(17) Lin, X. K.; Wang, Y. L.; Wu, L. X. *Langmuir* **2009**, *25*, 6081−6087.
(18) Wang, H. B.; Yan, Y.; Li, B.; Bi, L. H.; Wu, L. X. *Chem.—Eur. J.* **2011**, *17*, 4273−4282.
(19) Han, Y. K.; Zhang, Z. J.; Wang, Y. L.; Xia, N.; Liu, B.; Xiao, Y.; Jin, L. X.; Zheng, P.; Wang, W. *Macromol. Chem. Phys.* **2011**, *212*, 81−87.
(20) Polarz, S.; Smarsly, B.; Antonietti, M. *Chem. Phys. Chem* **2001**, *2*, 457−461.
(21) Stein, A.; Fendorf, M.; Jarvie, T. P.; Müller, K. T.; Benesi, A. J.; Mallouk, T. E. *Chem. Mater.* **1995**, *7*, 304−313.
(22) Landsmann, S.; Lizandara-Pueyo, C.; Polarz, S. *J. Am. Chem. Soc.* **2010**, *132*, 5315−5321.
(23) Giner-Casares, J. J.; Brezesinski, G.; Möhwald, H.; Landsmann, S.; Polarz, S. *J. Phys. Chem. Lett.* **2012**, *3*, 322−326.
(24) Bu, W.; Uchida, S.; Mizuno, N. *Angew. Chem., Int. Ed.* **2009**, *48*, 8281−8284.
(25) Lin, X.; Liu, F.; Li, H.; Yan, Y.; Bi, L.; Bu, W.; Wu, L. *Chem. Commun.* **2011**, *47*, 10019−10021.
(26) Yelamanchili, R. S.; Walther, A.; Müller, A. H. E.; Breu, J. *Chem. Commun.* **2008**, 489−491.
(27) Lee, J.; Orilall, M. C.; Warren, S. C.; Kamperman, M.; Disalvo, F. J.; Wiesner, U. *Nat. Mater.* **2008**, *7*, 222−228.
(28) Liu, S.; Tang, Z. *Nano Today* **2010**, *5*, 267−281.
(29) Lunkenbein, T.; Rosenthal, D.; Otremba, T.; Zihui, L.; Sai, H.; Bojer, C.; Trunschke, A.; Wiesner, U.; Schlögl, R.; Breu, J. To be submitted.
(30) Brinker, C. J.; Lu, Y. F.; Sellinger, A.; Fan, H. Y. *Adv. Mater.* **1999**, *11*, 579−585.
(31) Templin, M.; Franck, A.; Du Chesne, A.; Leist, H.; Zhang, Y.; Ulrich, R.; Schädler, V.; Wiesner, U. *Science* **1997**, *278*, 1795−1798.
(32) Schacher, F.; Müllner, M.; Schmalz, H.; Müller, A. H. E. *Macromol. Chem. Phys.* **2009**, *210*, 256−262.
(33) Nakamura, O.; Ogino, I.; Kodama, T. *Solid State Ionics* **1981**, *3−4*, 347−351.
(34) Förster, S.; Burger, C. *Macromolecules* **1998**, *31*, 879−891.
(35) Förster, S.; Timmann, A.; Konrad, M.; Schellbach, C.; Meyer, A.; Funari, S. S.; Mulvaney, P.; Knott, R. *J. Phys. Chem. B* **2005**, *109*, 1347−1360.
(36) Luo, C.; Liu, Y.; Li, Z. *Soft Matter* **2012**, *8*, 2618−2626.
(37) Kozhevnikov, I. V. *Chem. Rev.* **1998**, *98*, 171−198.
(38) Mei, Y.; Lauterbach, K.; Hoffmann, M.; Borisov, O. V.; Ballauff, M.; Jusufi, A. *Phys. Rev. Lett.* **2006**, *97*, 158301.
(39) Plamper, F. A.; Walther, A.; Müller, A. H. E.; Ballauff, M. *Nano Lett.* **2007**, *7*, 167−171.
(40) Bernheim-Groswasser, A.; Wachtel, E.; Talmon, Y. *Langmuir* **2000**, *16*, 4131−4140.
(41) Jain, S.; Bates, F. S. *Science* **2003**, *300*, 460−464.
(42) Bang, J.; Jain, S.; Li, Z.; Lodge, T. P.; Pedersen, J. S.; Kesselman, E.; Talmon, Y. *Macromolecules* **2006**, *39*, 1199−1208.
(43) Jain, S.; Gong, X.; Scriven, L. E.; Bates, F. S. *Phys. Rev. Lett.* **2006**, *96*, 138304.
(44) Garcia, B. C.; Kamperman, M.; Ulrich, R.; Jain, A.; Gruner, S. M.; Wiesner, U. *Chem. Mater.* **2009**, *21*, 5397−5405.
(45) Kamperman, M.; Fierke, M. A.; Garcia, C. B. W.; Wiesner, U. *Macromolecules* **2008**, *41*, 8745−8752.
(46) Aoshima, A.; Tonomura, S.; Yamamatsu, S. *Polymer. Adv. Tech.* **1990**, *2*, 127−132.
(47) Rocchicciolideltcheff, C.; Fournier, M.; Franck, R.; Thouvenot, R. *Inorg. Chem.* **1983**, *22*, 207−216.
(48) Rocchicciolideltcheff, C.; Aouissi, A.; Bettahar, M.; Launay, S.; Fournier, M. *J. Catal.* **1996**, *164*, 16−27.
(49) Chiu, J. J.; Kim, B. J.; Kramer, E. J.; Pine, D. J. *J. Am. Chem. Soc.* **2005**, *127*, 5036−5037.
(50) Lin, Y.; Böker, A.; He, J.; Sill, K.; Xiang, H.; Abetz, C.; Li, X.; Wang, J.; Emrick, T.; Long, S.; Wang, Q.; Balazs, A.; Russell, T. P. *Nature* **2005**, *434*, 55−59.
(51) Kim, B. J.; Fredrickson, G. H.; Bang, J.; Hawker, C. J.; Kramer, E. J. *Macromolecules* **2009**, *42*, 6193−6201.
(52) Kim, B. J.; Bang, J.; Hawker, C. J.; Chiu, J. J.; Pine, D. J.; Jang, S. G.; Yang, S. M.; Kramer, E. J. *Langmuir* **2007**, *23*, 12693−12703.
(53) Jang, S. G.; Kim, B. J.; Hawker, C. J.; Kramer, E. J. *Macromolecules* **2011**, *44*, 9366−9373.

(54) Shearman, G. C.; Ces, O.; Templer, R. H.; Seddon, J. M. *J. Phys.: Condens. Matter* **2006**, *18*, S1105−S1124.
(55) Shearman, G. C.; Tyler, A. I. I.; Brooks, N. J.; Templer, R. H.; Ces, O.; Law, R. V.; Seddon, J. M. *Liq. Cryst.* **2010**, *37*, 679−694.